Mathematical Model of a Pneumatic Conveying Dryer

Christian Fyhr and Anders Rasmuson
Dept. of Chemical Engineering Design, Chalmers University of Technology, S-412 96 Gothenburg, Sweden

A model for a pneumatic-conveying dryer is presented, with the focus on the superheated steam drying of wood chips, although it can also be used for other porous materials and drying media. It includes a comprehensive 2-D model for the drying of single wood chips, which accounts for the main physical mechanisms occurring in wood during drying, including coupled transport of water, air, vapor and heat. This model allows for features such as initial condensation and flashing at the outlet, as well as the falling rate period when the drying is controlled by internal transport. External drying conditions in the dryer are calculated by applying mass, heat and momentum equations for each incremental step in dryer length. A plug-flow assumption is made for the dryer model, and single-particle and dryer models were solved iteratively. The irregular movement and nonspherical shape of wood chips are accounted for by measuring drag and heat-transfer coefficients.

Model calculations illustrate the complex interactions among steam, particles, and walls that occur in a flash dryer. The drying rate, the slip velocity, and temperature vary in a complex manner through the dryer, necessitating the use of a comprehensive single-particle model, as in this case. Previous experimental data on the drying of bark chips in a pilot dryer was used to verify the model. The predicted temperature and pressure profiles, as well as the final moisture content of the material, agreed well with the measurements. Thus, the model provides a useful tool for the design and scale-up of pneumatic-conveying dryers. Effects of steam and material properties on the drying were investigated with different design parameters.

Introduction

Pneumatic-conveying dryers, also known as flash dryers, are one of the most common types of industrial dryer. In a pneumatic-conveying dryer, the external conditions for the particles vary in the direction of flow. The pressure of the drying medium decreases due to friction between the gas and the walls as well as to momentum losses caused by the acceleration of the particles. The temperature is affected by heat transfer to the particles (drying) and heat transfer at the wall. The slip velocity between the particles and the gas is controlled by the interfacial drag and friction between the particles and the walls. Thus, all three relevant external parameters that control the drying rate vary considerably along the dryer.

Kemp et al. (1991) have reviewed models for pneumatic-conveying dryers and concluded that none have been entirely successful. In the same article, a new model was developed and tested experimentally. In this model, as in previous ones, the drying rate of the single particles was assumed to be constant or modeled by simple, characteristic drying curves. The main drawbacks of the characteristic curve concept are, first, that the critical moisture content at which the drying rate starts to decrease is assumed to be constant and, second, that the drying rate thereafter is a function of the moisture content only. This may be a good assumption for mild drying conditions, but the intense heat-transfer rate in dryers of the present type leads to a drying sequence that is controlled by internal transfer to the surface during the main part of the drying process. The critical moisture content and the drying rate thereafter become, under these conditions, functions of

Correspondence concerning this article should be addressed to A. Rasmuson.

both the internal and external characteristics of the particle. This suggests that a more comprehensive model for the single particle is needed. The aim of this study is to develop a one-dimensional model for heat, mass, and momentum transport along the dryer. External, as well as internal, conditions for single-particle drying are accounted for.

The Pilot Dryer

The pilot dryer at the Department of Chemical Engineering, Chalmers University of Technology (CTH), is depicted in Figure 1. The dryer loop has a total length of 200 m and is divided into six erect sections with uprisers and downcomers. The inlet steam velocity can be varied between 15 and 30 m/s, depending on the size and density of the material to be dried. The pressure of the conveying steam can be varied between 0.2 to 0.6 MPa. The feed is introduced by means of a rotary valve and is conveyed by the steam through the dryer, giving a residence time ranging between 10 and 40 s, depending on the steam velocity and material. The dry product is separated at the outlet in a cyclone and is discharged through a rotary valve. The steam is recirculated by two fans and the surplus steam from the drying is bled off. This surplus steam can either be used as a heating medium in another process or recompressed and reused in the dryer itself. The first seven tubes and upriser No. 6 are equipped with heat exchangers where high-pressure steam (0.9–1.5 MPa) heats the conveying steam externally. The inlet steam temperature can be as high as 200°C if an extra superheater is used. The tube diameter is 100 mm in the heat exchangers and 150 mm elsewhere. The performance and different experimental data of the pilot dryer for several different materials were reported earlier by Hilmart and Grén (1987). The dimensions used in the simulations and the conditions of the conveying steam reflect those in the pilot dryer, and the simulated results are compared with actual running data.

Single-particle Model

Recently, a model for drying porous, anisotropic materials with specific application to wood was developed (Fyhr and Rasmuson, 1996a). The work was based on the drying of wood

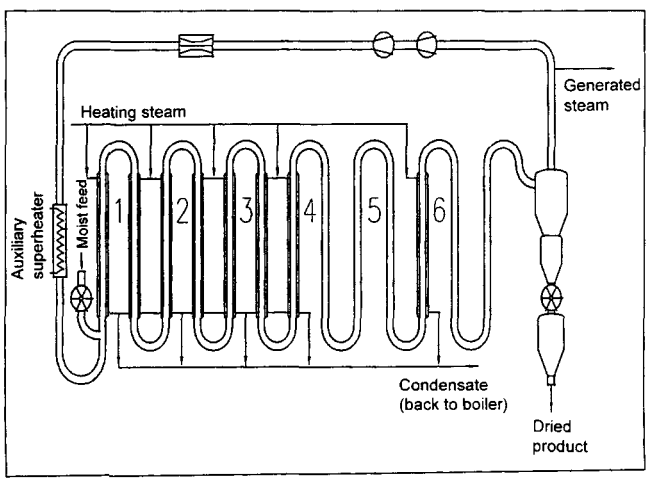

Figure 1. Pilot dryer.

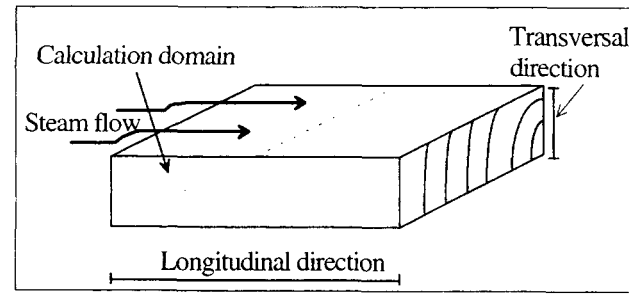

Figure 2. Wood chip.

chips, although the model can be used for the drying of other porous, hygroscopic materials with relevant sets of material data. The shape of the wood chip upon which the simulations and experiments were based is depicted in Figure 2. The chip is treated as being stationary, with steam flowing past, as indicated.

The mathematical details of the single-particle model are given along with the transport coefficients in Appendix A. Three moisture phases were accounted for: free (liquid) water; bound water; and water vapor. The model is two-dimensional (longitudinal and transversal direction) in order to account for the strong anisotropicity of wood. The coupled flow of water, air and steam is modeled by an extended Darcy's law. The diffusion of bound water is modeled by a Fick law expression. Heat is transported internally by convection and conduction, and external heat transfer to the surface occurs via convection and radiation. The model can cope with a wide range of external conditions such as high temperatures and pressures of steam above the atmospheric. A code written for geothermal applications, developed by Pruess (1987), formed the basis for the work. This code, called TOUGH, includes general features for transport in porous media and, with some modifications and extensions, it could be used to simulate the drying of wood.

Experiments for the two most common softwoods (pine and spruce) at a wide range of external conditions were performed in order to validate the single-particle model. The equipment enabled simultaneous measurements of the average moisture content, as well as the temperature and pressure, at the center of the chip. All simulations were performed prior to the experiments and all transport parameters were taken from the literature. A comparison between the experiments and calculations showed good agreement. All experimentally observed physical features of drying were predicted well by the simulations. Thus, based on this work, it can be concluded that the different physical transport mechanisms and the parameters therein used in the model, are valid. It is therefore expected that, in comparison with simplified models (e.g., characteristic curve model), this model is more suited for predicting drying rates at conditions beyond the range for which controlled experiments are available.

A more recent investigation, with emphasis on the drying conditions present in a pneumatic-conveying dryer, was performed (Fyhr and Rasmuson, 1996b) where different sizes of wood chips and various wood species were studied. The effect of varying the inlet temperature of the chips (preheating) and the flashing effect at the outlet as the pressure drops (postdrying) were investigated.

Hydrodynamic Model for the Dryer

The main assumptions made in the hydrodynamic-dryer model are:

- Plug flow is 1-D.
- No particle–particle interactions occur.
- The flow is steady.

The following reasoning was made regarding the first assumption: For this system, the axial direction is the most important one, since the length-scale ratio L/D is very large (around 2000). The mixing of momentum and heat is very rapid in the cross section of the tube due to the high degree of turbulence ($Re_D > 10^5$), which leads to flat radial profiles of heat and velocity.

The variation of the particle velocity in the radial direction is very small, according to the experimental investigation by Lee and Durst (1982). They also concluded that there is a tendency for the radial particle-velocity profiles to flatten out as the particle size increases. The particles used by Lee and Durst were much smaller ($d_p < 0.8$ mm) in comparison with the particles used here ($d_p > 5$ mm). A mathematical model for pneumatic conveying, which included the radial variation of the axial velocity, was developed by Adewumi and Arastoopour (1986). They implied a no-slip condition at the wall for the particles, which led to a clear simulated radial-velocity profile. Comparison with experimental data showed large discrepancies, and they concluded that the no-slip condition at the wall was not appropriate. Accordingly, it was concluded that radial distributions of gas and particle velocities are insignificant and that a one-dimensional (1-D) (axial direction) model for the dryer is sufficient to calculate relevant external conditions for the single particle along the dryer.

The concept of "mean free path for molecules" (the average distance between collisions) was used in order to investigate the importance of particle–particle interactions (second assumption). This theory was used by Gidaspow (1994) to obtain a dependence of the mean free path for particles in conveying of dilute particle suspensions as:

$$l = \frac{1}{6\sqrt{2}} \frac{d_p}{\epsilon_s}. \tag{1}$$

If the particle diameter is assumed to be on the order of 0.005 m and the solids voidage 0.001 (typical average value in the dryer), the mean free path becomes about 0.6 m, which leads to the conclusion that wall collisions are far more important than particle–particle collisions.

The third assumption that the flow is steady is justified since the dryer is to be run in a continuous manner and the time derivatives are only of interest for start-up and control purposes.

The mass and energy balances are written according to standard formulation (Gidaspow, 1994), and the momentum balances are written with Eularian notation, which in this case is analogous to the Lagrangian formulation.

The balances of mass, heat, and momentum are

Mass balance for the gas phase

$$\frac{d(\epsilon_g \rho_g v_g)}{dz} = \dot{m}. \tag{2}$$

Mass balance for the solid phase (based on the solid inert part)

$$\frac{d(\epsilon_{p,i} \rho_s v_{p,i})}{dz} = 0. \tag{3}$$

Energy balance for the gas phase

$$\frac{d(\epsilon_g \rho_g v_g H_g)}{dz} = \dot{q} + \dot{q}_w. \tag{4}$$

Momentum balance for the gas phase

$$\int\int \rho_g v_g (\boldsymbol{n} \cdot \boldsymbol{v}_g)\, dA = \Sigma F = F_D + F_g + F_{wf} + F_P, \tag{5}$$

where

$$F_D = -\Sigma n_i \frac{1}{2} C_{D,i} A_{p,i} \rho_g (v_g - v_{p,i}) \mid v_g - v_{p,i} \mid \quad \text{(particle drag)} \tag{6}$$

$$n_i = \frac{\epsilon_i dz \frac{1}{4} \pi D^2}{V_{pi}} \tag{7}$$

$$F_g = -Adz\epsilon_g \rho_g g \quad \text{(gravitation)} \tag{8}$$

$$F_{wf} = -\frac{1}{2} \pi D dz f \rho_g v_g^2 \quad \text{(wall friction)} \tag{9}$$

$$F_P = -AdP \quad \text{(pressure force)}. \tag{10}$$

Momentum balance for the solid phase

$$\int\int \rho_{p,i} v_{p,i} (\boldsymbol{n} \cdot \boldsymbol{v}_{p,i})\, dA = \Sigma F_i = F_{D,i} + F_{g,i} + F_{wf,i}, \tag{11}$$

where

$$F_{D,i} = n_i \frac{1}{2} C_D A_p \rho_g (v_g - v_p) \mid v_g - v_p \mid \quad \text{(particle drag)} \tag{12}$$

$$F_{g,i} = -n_i V_{p,i} \rho_{p,i} g \quad \text{(gravitation)} \tag{13}$$

$$F_{wf,i} = -n_i \frac{1}{2} f_P V_{p,i} \rho_{p,i} v_{p,i}^2 / D \quad \text{(wall friction)}. \tag{14}$$

The forces other than inertia due to acceleration, which are often encountered in the literature of two-phase fluid dynamics, are the so-called "added mass" and "Basset" forces (Clift et al., 1978). These forces can be shown to be neglibile in the present case (Appendix B).

The equations were discretized by dividing the length of the dryer into small segments, each with a length of Δz. A set of five nonlinear algebraic equations were then obtained that are linearized and solved iteratively according to Newtons method. Typically, Δz was chosen to be on the order of 0.02 m, giving about 10,000 control volumes. The accuracy of the solution was checked by decreasing Δz: the solution only changed in the fourth decimal when Δz equalled 0.002 m.

Constitutive equations

The volume fraction of gas in each segment is denoted by ϵ_g and the solid volume fraction by ϵ_{pi}. The sum of these is unity and, if more than one particle size of solid is present, the relation is

$$\epsilon_g + \sum_{i=1}^{n} \epsilon_{pi} = 1. \tag{15}$$

One additional relation is necessary in order to close the set of equations. This is the relation between the gas density and the pressure and temperature of the steam according to

$$\rho_g = z \frac{M_g P_g}{RT} \quad \text{with} \quad z = 1.019. \tag{16}$$

Boundary Conditions

Inlet conditions

The inlet conditions include:

- Steam velocity
- Steam temperature
- Steam pressure
- Particle feed rate
- Inlet conditions of the chips (temperature and moisture content)

Boundary conditions at the wall

Walls and Gas. The term $\dot{q}_w$ in Eq. 4 represents the heat transfer between the gas and the walls and is calculated as

$$\dot{q}_w = 4h(T_w - T_g)/D, \tag{17}$$

where h is the heat-transfer coefficient, which is calculated according to Welty et al. (1984):

$$Nu_D = 0.023 Re_D^{0.8} \mathrm{Pr}^{0.4} \qquad Re_D > 10^4, \tag{18}$$

where T_w is set at the saturation temperature of the heating steam. In the absence of external heat exchangers, the overall heat-transfer coefficient between the gas and the surroundings is set at 2 W/m^{2}K, and T_w is the temperature of the surroundings (= 20°C). The friction factor f in Eq. 9 is taken from the experimental data for the pilot dryer obtained by Hilmart and Grén (1987) to be 0.015.

Walls and Particles. The only included heat-transfer mechanism between the walls and particles is radiation according to Stefan Boltzmann law:

$$q_{\mathrm{rad}} = e\sigma(T_w^4 - T_s^4), \tag{19}$$

where the emissivity e is set at 0.9 and σ is the Stefan Boltzmann constant. Conductive heat transfer caused when particles bounce against the wall is assumed to be negligible.

The friction between the walls and particles is included according to Eq. 14, where the friction factor for the particle–wall interactions f_p is extracted from the work by Yang (1978):

$$f_p = A \frac{(v_g - v_p)_{ss}}{v_{p,t}} \qquad \begin{cases} A = 0.0126 & v_g \geq 1.5 v_{p,t} \\ A = 0.0410 & v_g \leq 1.5 v_{p,t}, \end{cases} \tag{20}$$

where $v_{p,t}$ is the terminal velocity for an isolated particle. This correlation was based on spherical particles ranging between 0.1 to 4 mm, and it is dubious whether it is applicable to nonspherical, larger particles, as in this case. However, due to the lack of other experimental data, Eq. 20 was used.

In the bends, the particles are expected to interact more with the walls than in vertical flow. It is assumed that the particles slide around the bend, and the friction coefficient between the particles and pipe material is then important. The forces that constitute the normal force are, then, the centripetal force and gravity. The friction force between the particles and walls can then be written as

$$F_b = \mu V_p \rho_p \left(g \sin \alpha + \frac{v_p^2}{R_b} \right), \tag{21}$$

where μ is the friction coefficient, R_b is the bend radius, and α is the angle that defines the position of the particle in the bend (at the entrance: $\alpha = 0°$ and at the outlet $\alpha = 180°$). The gravity constant is set positive in the lower bends and negative in the upper bends. This formulation leads to a smaller bend friction in the upper bends than in the lower bends due to the different directional action of gravity. As the chips slide around the bend, their orientation is restricted, and consequently they exhibit a much smaller projected area than in normal flow: this leads to a significant reduction of the drag in the bends. The projected area in the bends is therefore calculated as the thickness times the average length of the chips $[0.5T(L + W)]$ instead of the average area. By inserting the value 0.75 for the friction coefficient, the residence time equals the measured ones. This is in fact the only fitted parameter in the entire model, including the single-particle model.

Boundary conditions between the gas and solids

The particulate and gas phases interact by exchanging heat, momentum, and mass. The interaction of mass (i.e., drying) is determined from the single-particle model by inserting the boundary condition from the dryer model. The temperature of the surrounding steam is known: the heat transfer to the particle can then be determined if the heat-transfer coefficient is also known. Several correlations for the heat-transfer coefficient for heat transfer between particles and fluids can be found in the literature. These are, however, almost exclusively based on spherical particles for which orientation in space is irrelevant. Very few correlations for heat transfer to nonspherical particles such as wood chips were found. Wood chips flow in an irregular manner and with unknown orientation in space, which makes theoretical estimation of the heat-transfer coefficient extremely difficult. The slip velocity between particle and steam is determined from the momentum balance: the interaction parameter here is the drag coefficient. Again, most of the drag coefficients found in the literature are based on spheres, although some investigations on irregular particles were also found. None of these matched the geometry of the wood chips in this investigation exactly,

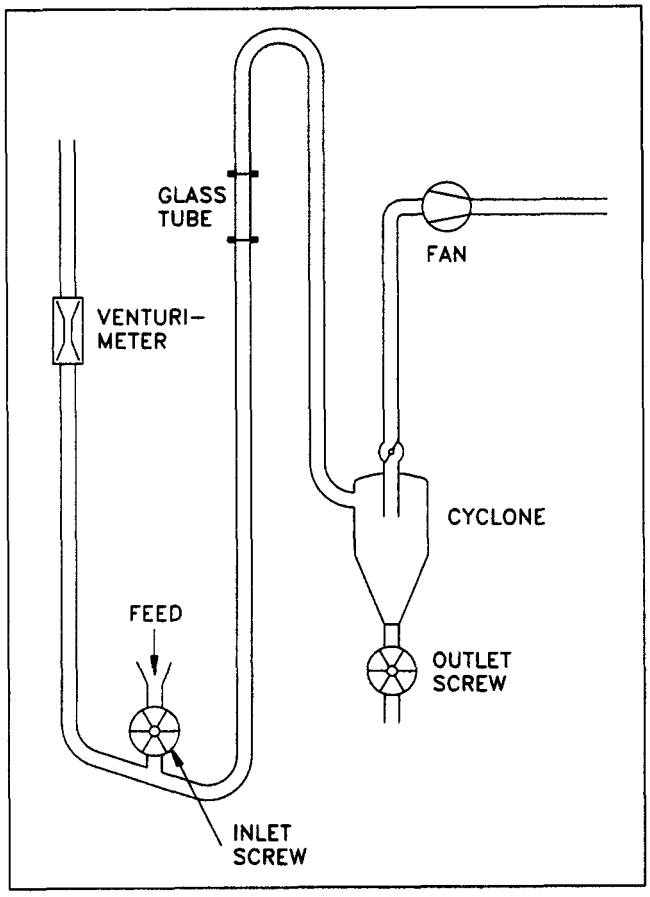

Figure 3. Small-scale pilot dryer.

however. They were also made for stationary particles with fixed orientation. Due to the irregular motion of the wood chips in the dryer, the projected area is also unknown, which makes the interpretation of the literature values difficult. Thus, due to the lack of relevant data for these interaction parameters, some preliminary dynamic experiments were performed.

Drag Coefficients. The drag coefficient determines the slip velocity and the residence time in the dryer: a decrease of this coefficient leads to higher values of both. This, in turn, enhances drying significantly. It is, therefore, of great interest to have accurate values of this coefficient. It is expected that, for the high range of slip velocities that are employed here, the value of C_D is independent of the Reynolds number (Newtons regime). A small-scale pilot dryer (depicted in Figure 3) was used for the experimental determination of the drag coefficients under nondrying conditions. The height of the dryer was 11 m and a glass tube was inserted in the top part of the upriser. The velocity of the gas was measured by a venturimeter. A video camera was used to follow the particles as they passed the transparent section so that the velocity of the particles could be measured. The drag coefficients were then calculated by applying a force balance on the chips:

$$mg = \frac{1}{2} C_D A_p \rho_g v_{\text{slip}}^2 - \frac{1}{2} f_p m_p v_p^2 / D. \tag{22}$$

The second term on the righthand side represents the wall friction between the particles and the walls, as in Eq. 14. The particle velocity varied considerably, even for particles under identical conditions, which made several tests for each case necessary. About 15 runs gave a stable mean value of the particle velocity and the standard deviation was about 15% of the mean value. The large standard deviation is explained by the irregular motion of the particles and the randomized interaction with the walls. The secondary motion, which was recorded by the video camera, included both tumbling and rotation around the chip's symmetry axes. The projected area then changed in the flow direction, which led to different local projected areas and, therefore, different drag forces on the chip. The total residence time in the dryer was also measured. The standard deviation here was much smaller, which indicates that the local differences in the particle velocity is averaged out to some extent. Several different particle sizes and materials were used and the resulting drag coefficient became:

$$C_D = 2.33 \pm 0.30. \tag{23}$$

There was no significant influence of density, size, or slip velocity on the drag coefficient. The projected area was chosen to be the average area calculated as

$$A_p = (L \times T + L \times W + T \times W)/3. \tag{24}$$

If the area is based on the projected area of a sphere of equal volume, the standard deviation is somewhat larger ($C_D = 3.2 \pm 0.75$). Since the standard deviation is larger with this projected area, the average area is more suitable for use in this case.

As mentioned earlier, there is some work on the drag coefficients in the literature. It is interesting to compare these with the values found here: Table 1 shows some values that can be found. All values are within the standard deviation of the present result. The measured drag coefficient is specific for this system since the wall friction factor is uncertain. It is therefore not advisable to use the value for free stream flow. An error analysis (see Appendix C) gives the error in the drag coefficient as the friction factor is changed.

Heat-transfer Coefficients. The heat-transfer coefficients were measured by inserting hot aluminum and magnesium chips in the same small-scale pilot dryer as described previously. The metal chips were preheated to 100°C and then conveyed through the tubes of the dryer by means of cold air (20°C). The chips were inserted one by one, ensuring a constant air temperature through the tube. The total energy of the chip after the dryer was measured in a simple calorimeter consisting of an isolated cup containing 20 mL of toluene.

Table 1. Comparison of Measured C_D with Data from the Literature

Source	C_D	Comment
This work	3.2 ± 0.75	Experimental
Haider and Levenspiel (1988)	3.6	Based on sphericity
Pettyjohn and Christiansen (1948)	2.5	Experimental value for L, W, T = 4,4,1 mm
Pettyjohn and Christiansen (1948)	2.9	Based on sphericity

The toluene was stirred by a small magnetic stirrer, and its temperature response was measured by a thermocouple. The heat-transfer coefficient was then calculated by the heat balance:

$$h = \frac{mCp}{A\theta} \ln\left(\frac{T_{out} - T_\infty}{T_{in} - T_\infty}\right), \tag{25}$$

where m is the mass of the chip, and θ is the residence time. The radiative contribution to the heat transfer is negligible in this case (see Appendix D). Square metal chips were used and the length was varied between 8 and 30 mm and the thickness between 0.5 and 4 mm. The air velocity was varied between 16 and 18 m/s. The average slip velocity between the gas and the chip in the tube was calculated by simply dividing the length of the tube by the residence time of the chip. The measured heat-transfer coefficients were correlated to the following equation:

$$h = 3.3(v_{slip})^{0.79} T^{-0.41} L^{-0.65} \rho^{-0.34} \qquad v_{slip} = |v_g - v_p| \tag{26}$$

The exponent for the slip velocity is in the order of 0.8, which is often encountered in the literature for heat transfer to particles at high Reynold numbers (e.g., Bandrowski and Kaczmarzyk, 1978). The dimensions of the chip have a strong influence on the heat transfer, as indicated by the exponents -0.65 for the length and -0.41 for the thickness. Heat transfer is consequently enhanced by decreasing the dimensions of the chip. The density also has a significant effect due to its influence on the chip motion, as discussed below.

It is of interest to compare the measured heat transfer coefficients with correlations that are found in the literature. The correlations chosen were:

$$Nu = 2 + 0.6 Re^{0.5} Pr^{0.33} \tag{27}$$

$$Nu = 2 + (0.4 Re^{0.5} + 0.06 Re^{0.75}) Pr^{0.4} \left(\frac{\mu_\infty}{\mu_0}\right)^{0.25} \tag{28}$$

$$St = \frac{h}{\rho v_{slip} C_p} = 0.106 Re_L^{-0.25}. \tag{29}$$

The first correlation (Ranz and Marshall, 1952) was obtained from experiments on the evaporation of water droplets and is very commonly used for heat transfer to particles. The second (Whitaker, 1972) is used for larger particles at high Reynolds numbers, where the effect of turbulence is accounted for by the term proportional to $Re^{0.75}$. The third correlation (Sorenson, 1969) was obtained from mass-transfer experiments on truncated slabs of naphthalene, and includes the effect of a recirculation loop at the leading edge, which enhances the transfer. The first two are based on the diameter of a sphere and the third on the length of the chip. A comparison with the present results was made by using the diameter of a sphere with a volume equal to the chip as characteristic lengths in Eqs. 27 and 28. The results show that all three correlations significantly underestimated the heat-transfer coefficient under the present conditions. The first gave values of h that were, on average, 42% of the measured ones. The values for the other two were 50% and 48%, respectively. There was a tendency for the deviation between these correlations and the present measurements to increase as the chip size decreased. The values found in this investigation are then about a factor of 2 higher than those given from conventional correlations. This is expected to be due to a secondary motion of the chips that is enhanced by a low moment of inertia (i.e., small size and low density). This leads to a surface renewal that enhances the heat transfer. Since the measured heat-transfer coefficients are valid for this specific system only, it is not meaningful to correlate the measured values with a Nusselt number correlation.

Complete Dryer Model

A complete dryer model is obtained by combining the hydrodynamic dryer model with the single-particle model. The coupling between the models appears in the hydrodynamic model as the source terms of mass and energy, $\dot{m}$ and $\dot{q}$, due to drying. The model for the single particle is very complex and requires long computing times, which makes a direct solution of the coupled model difficult. An iterative approach is used instead, as illustrated in Figure 4. The dryer model is solved first with assumed values of $\dot{m}$ and $\dot{q}$ as functions of residence time for the particle. The output from the dryer model is vectors containing the temperature, pressure, and slip velocity as functions of particle residence time. These vectors are then inserted as transient boundary conditions into the single-particle model. New values of $\dot{m}$ and $\dot{q}$ are then obtained and a new computation of the dryer model gives updated boundary conditions; these are then used in the single-particle model and so forth until convergence is achieved. Convergence is defined as when the values for the temperature, slip velocity, and pressure no longer change in the second decimal, which normally requires three iterations.

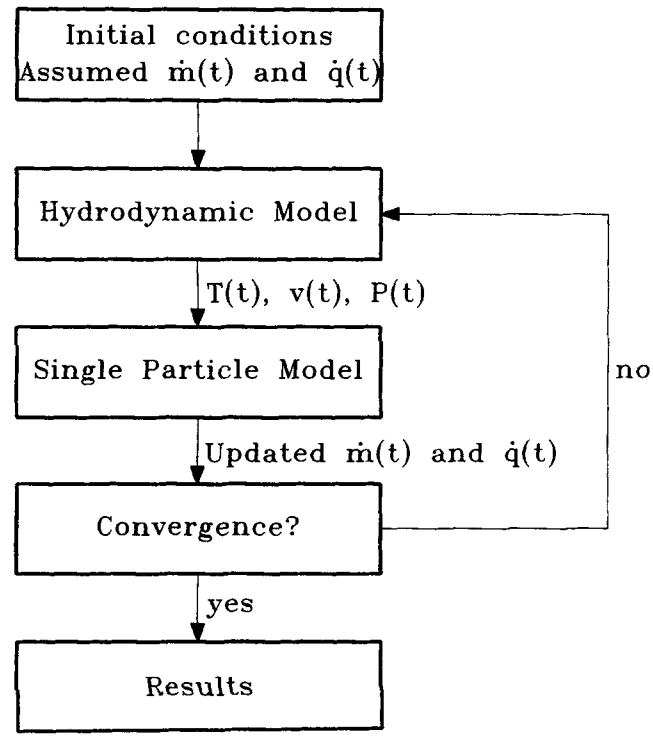

Figure 4. Flow chart for the complete dryer model.

Model Validation

An extensive experimental investigation on the drying of bark chips in the pilot dryer was performed by Hilmart and Grén (1987), who measured the temperature profile, overall pressure drop, and the final moisture content of the dried bark. Although bark is not the same material as wood chips, some similarities exist that lead to a drying sequence comparable with pine wood. Bark is more porous than wood and, to compensate for this, the porosity in the single-particle model was changed from 0.67 and 0.75. In order to validate the model, a simulation of drying bark chips under the following conditions was performed:

- Initial temperature of the bark chips = 25°C
- Initial moisture content = 1.62 kg water/kg solid
- Dimensions (L, T, W) = 0.02, 0.002, 0.01 m
- Permeabilities $K_L = 1 \times 10^{-12}$ m^2
  $K_T = 1 \times 10^{-15}$ m^2
- Feed rate (dry solid) = 0.05 kg/s (= 173 kg/h)
- Initial steam velocity = 20 m/s
- Initial steam temperature = 205°C
- Initial steam pressure = 2.6 bar
- Saturation temperature of heating steam = 180°C

The resulting profiles of moisture content, temperature, slip velocity, and steam pressure are depicted in Figures 5 and 6.

The slip velocity varies considerably throughout the dryer. The highest slip velocities are found at the inlet and after the bends where the chips are accelerated. The different directional action of gravity, however, results in a higher slip velocity in the uprisers than in the downcomers. In tower No. 3 the diameter of the tube is increased from 10 cm to 15 cm. As a result, the gas velocity decreases by a factor of 2.25. The slip velocity then decreases, and is actually reversed in the downcomers where the particles have a higher velocity than the gas. There are, therefore, points in downcomers 3 to 6 where the slip velocity is zero, as seen in Figure 5.

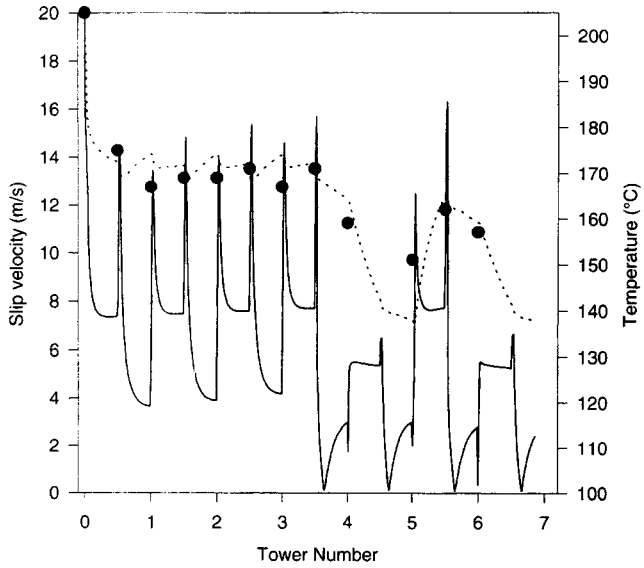

Figure 5. Slip velocity and temperature along the dryer: ----calculated temperature; ● measured temperature; —calculated slip velocity.

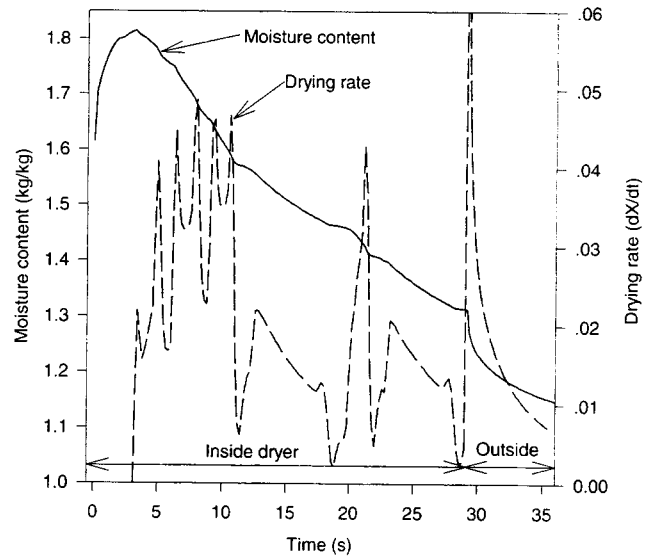

Figure 6. Moisture content and drying rate as functions of time.

The temperature drops approximately 35°C during the first second due to the insertion of wet and cold material. The temperature then approaches the saturation temperature of the heating steam (180°C), but drops, due to heat losses, in the part of the dryer that is not equipped with heat exchangers. The last heat exchanger, in upriser No. 6, heats the steam to 160°C. The temperature drops again in the final part of the dryer. The oscillations in the temperature profile between towers 1 and 3 are the result of the different drying rates in uprisers and downcomers. The steam is heated in the downcomers due to the low drying rate and cooled in the uprisers where the drying is more intense. The measured temperature profile is in good agreement with the simulated one. The low frequency of measuring points means that the dip in the temperature between towers 4 and 5 is not fully covered. The simulated pressure drop is approximately 25 kPa through the dryer, which is confirmed by the measurements.

The moisture content and drying rate as functions of chip residence time are depicted in Figure 6. The moisture content increases initially as a consequence of the condensation of steam on the surface and within the particle. This effect is very pronounced since the bark is not preheated at all. This leads to the drastic effect that almost half of the dryer length is required just to reattain the initial moisture content. The curve for the drying rate is similar to the slip velocity profile in Figure 5. This is due to the fact that the slip velocity strongly affects the heat transfer according to Eq. 26. The drying rate is significantly lower in the part of the dryer with 15-cm tubes because of the low slip velocities and temperatures. This part of the dryer hardly contributes to the overall drying at all. The disadvantageous effect of initial condensation is partly compensated for by flashing at the outlet, where the pressure drops from 2.5 bar to 1 bar, thus reducing the moisture content by approximately 0.15 kg/kg in less than 5 s. The measured final moisture content is about 10% or 0.1 kg/kg lower than the simulated one. This minor discrepancy has at least two explanations. First, the stated dimensions of the chips represent assumed average values extracted from

the source (Hilmart and Grén, 1987). It can be suspected that these values are in the higher end of the distribution since smaller particle sizes are likely to be present due to the cutting process. This leads to an average higher measured drying rate. Second, drying in the cyclone is not included in the calculations.

Effect of Varying Different Design Parameters

As could be seen in the previous section, the dryer does not work properly in all parts. Some modifications are therefore necessary if larger chips are to be dried in the dryer. First, the effect of initial condensation must be reduced, which is done by preheating the chips. Second, the extremely low slip velocities in the part with the 15-cm tubes can be avoided by treating all tubes as having the same diameter. Furthermore, the drying rate for bark is mainly controlled by external heat transfer. This may also be valid in the drying of pine chips; on the other hand, the other common softwood, spruce, is less permeable, so the internal resistance to mass transfer is more pronounced when this wood species is dried. In order to achieve an acceptable final moisture content of spruce chips, the following simulations were performed for a dryer length of 250 m instead. All tubes were treated as if they were equipped with heat exchangers in order to increase the steam temperature in the dryer. Real wood chips are often stored in large piles before drying; the initial moisture content is therefore significantly lower than for fresh bark and the value 0.7 kg/kg was used instead. The flashing effect at the outlet is omitted in the following calculations. This does not affect the comparisons, except for the effect of pressure. Thus, the following simulations were performed for chips of sapwood spruce at the following inlet conditions if nothing else is stated:

- Initial temperature of the wood chips = 80°C
- Initial moisture content = 0.7 kg water/kg solid
- Dimensions (L, T, W) = 0.025, 0.0025, 0.02 m
- Permeabilities: pine: $K_L = 1\times10^{-12}$ m^2; $K_T = 1\times10^{-15}$ m^2
  spruce: $K_L = 5\times10^{-13}$ m^2; $K_T = 1\times10^{-16}$ m^2
- Feed rate (dry solid) = 0.04 kg/s (= 144 kg/h)
- Initial steam velocity = 17 m/s
- Initial steam temperature = 200°C
- Initial steam pressure = 3.0 bar
- Saturation temperature of heating steam = 190°C

The results are presented in Table 2 where the residence time and final moisture content are given for the different cases.

Material properties

Effect of Different Wood Species (Spruce, Pine). The effect of different wood species is depicted in Figure 7. Their drying rates, however, are similar in the first part of the dryer, however, after about 7 s, the drying rate for spruce declines significantly. The surface of the spruce chip is then dry and the internal transport of moisture to the surface partly controls the drying rate. This leads to an increase of the surface temperature, and thus a lower heat transfer rate to the surface, resulting in a decreased drying rate. The drying rate is now a function of both the external drying conditions and the internal characteristics of the chip. The fact that the external conditions still affect the drying is obvious, since the drying rate curves still reflect the slip-velocity curve. The drying rate for pine is also lower in the final part of the dryer for the same reason. The drying rate for pine is, however, always equal to or larger than that for spruce. Consequently, the final moisture content is significantly lower for pine. The different residence times are a result of the varying densities of the wood chips. A spruce chip dries more slowly and has a higher average moisture content through the dryer than a pine chip. This leads to higher slip velocities and longer residence times. This partly compensates for the internal resistance to mass transfer.

Effect of Particle Size. Simulations for three different spruce-chip sizes were conducted in order to investigate the effect of particle size on drying. Drying is more intense for the smaller chips, which is due to the increased heat-transfer rate for the smaller chip. The heat-transfer experiments pre-

Table 2. Parameter Study

Size of Chips*	Vel. of Steam (m/s)	Temp.** (°C)	Steam Pres. (bar)	Tower Hgt. (m)	Res. Time of Chips (s)	Final Moist. Content
L	17	190	3	14	29	0.47
M	17	190	3	14	27	0.4
S	17	190	3	14	25.5	0.32
M	14	190	3	14	34	0.37
M	20	190	3	14	23	0.43
M	17	180	3	14	28	0.44
M	17	200	3	14	26	0.38
M	17	190	1	14	38	0.33
M	17	190	2	14	29.5	0.37
M	17	190	4	14	26	0.43
M	17	190	5	14	25	0.47
M	17	190	3	7	31	0.35
M	17	190	3	28	25	0.43

*L:(L, W, T) = 30, 24, 3 mm; M:(L, W, T) = 25, 20, 2.5 mm; S:(L, W, T) = 20.8, 16.7, 2.1 mm.
**Saturation temperature of the steam in the external heat exchangers.

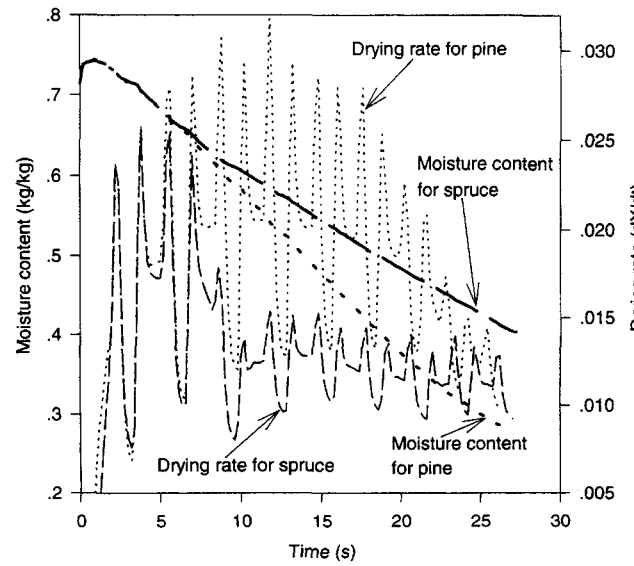

Figure 7. Effect of different wood species on drying.

sented in this work show that the heat-transfer coefficient is dependent on both slip velocity and the dimensions of the chip, according to Eq. 26. The higher mass of the larger chips leads to higher slip velocities and longer residence times, which partly compensate for the lower heat-transfer coefficients. It can be concluded that a longer dryer than the present one is necessary in order to achieve an acceptable final moisture content for the largest chip.

Effect of Particle-size Distribution. A feed that consisted of three different particle sizes in the same volumetric fractions was simulated in order to investigate the effect of particle-size distribution. The total feed rate and the particle sizes were the same as studied in the previous section. The calculation showed that the final moisture contents of the different chip sizes were almost the same as in the single-size calculations. Since particle–particle interactions are expected to be disregardable in this case, the only impact of a particle-size distribution is that the steam is affected, which influences drying indirectly. That is, the temperature and pressure profiles of the steam are different than in the drying of a single-sized feed. It can also be seen in the calculations that the effect is so small that drying is hardly affected at all. The average final moisture content is, however, changed. When dimensioning a dryer for a feed with a relatively narrow particle-size distribution, it is therefore sufficient to conduct calculations for the largest particle size. For a broad particle-size distribution, the effect will be more pronounced. An experimental investigation of the particle-size distribution is thus necessary. It is probable that more than three fractions must be considered to cover this phenomenon fully.

Steam properties

Inlet Steam Velocity. The inlet steam velocity was varied in order to study its effect on drying. Two main effects could be observed; first, the residence time decreased, and second, the final moisture content increased as the inlet velocity increased, as seen in Table 2. The first effect is due to the higher drag on the chips as the steam velocity increased. The increase in final moisture content is intimately connected to the lower residence time. A side effect of increasing the velocity is that the slip velocity increases, which leads to higher heat-transfer rates. Thus, the drying rate is higher for 20 m/s than for the other cases, and this partly compensates for the lower residence time. The mass flow of steam through the dryer increases due to the evaporation of water from the chips. Consequently, the steam velocity is higher in the final part of the dryer. As the inlet velocity decreases, the mass flow of steam also decreases. The steam is then more sensitive, which leads both to a lower steam temperature in the dryer as well as to a larger relative increase in steam velocity.

Effect of the Temperature of the Heating Steam. The effect on the residence time is relatively small as the temperature of the heating steam is changed. The temperature affects the drag in two ways: first, the density decreases as the temperature increases, which reduces the drag on the chips. Second, the lower density leads to a higher steam velocity, according to the continuity equation.

The most important effect of temperature on drying is, however, the change in driving force for heat transfer, as discussed in the next section. A decrease in temperature thus leads to a significantly higher final moisture content.

Inlet Steam Pressure. The inlet steam pressure also affects drying in several ways. The net result of increasing the pressure while keeping the other parameters constant is that the residence time decreases and the final moisture content increases. The reduced residence time is a result of the higher gas density caused by the increase in pressure, which, in turn, leads to higher drag on the chips.

The heat flux to the chips during the period of constant drying rate is given by

$$q = h(T_\infty - T_{sat}) = h\Delta T, \tag{30}$$

where ΔT represents the driving force for heat transfer. In this equation, the steam pressure affects the heat transfer coefficient, h, as well as the saturation temperature, T_{sat}, at the surface. Both these parameters increase as the pressure increases. The temperature of the steam, T_∞, also affects the heat flux. It is of interest to study the effect of both the pressure and temperature on the heat flux as depicted in Figure 8a and 8b, where the heat flux (normalized against the maximum value) is plotted. The slip velocity in Figure 8b is inversely dependent on the density, according to Eq. 12. It can be seen that an increase in steam temperature always increases the heat flux. For the case with fixed slip velocity (Figure 8a), an increase in pressure enhances the heat flux over the whole pressure range, at least at high temperatures. At lower temperatures, the decrease in driving force with pressure more than compensates for the increase in h. This leads to the inverse pressure dependency at low temperatures, as clearly seen in Figure 8a. In this type of dryer, a change in pressure or temperature also affects the slip velocity, and the resulting heat flux for this case is depicted in Figure 8b. Here, the heat flux at high temperatures has a maximum for a pressure of about 2 bar. For lower temperatures, however, the heat flux decreases as the pressure increases.

In addition to this heat-flux effect, the initial condensation becomes larger as the pressure increases. The net result is therefore that the final moisture content always increases with increased pressure (i.e., when the flashing effect at the outlet is not accounted for). It must also be kept in mind that the main advantage of steam drying, namely the reuse of the steam produced, is enhanced by high steam pressures.

Effect of different dryer designs

Height. While keeping the total dryer length constant, the height of the towers was varied. For a dryer with shorter towers, the chips negotiate the bends more often and the residence time as well as the average slip velocity increased significantly. This favors drying, as seen in Table 2. Drying is more intense in the bends than in the central parts of the uprisers and downcomers. The dryer should thus be constructed in a manner that takes this into consideration.

Dryer Diameter. The dryer diameter was doubled to investigate its effect on drying; the results are displayed in Figure 9. The most obvious effect is that the capacity is increased by a factor of 4. The volume fraction of solids is then the same as in the other cases. According to Eq. 14, the wall friction between the walls and particles is inversely proportional to the diameter and thus decreases as the diameter is doubled.

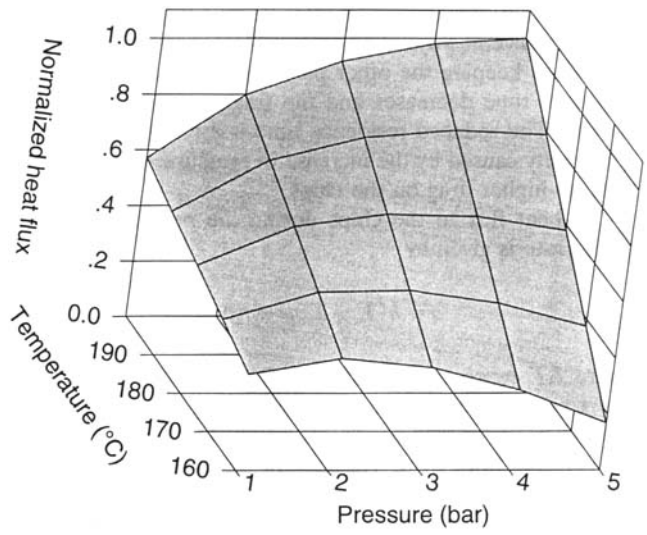

Figure 8a. Heat flux at fixed slip velocity.

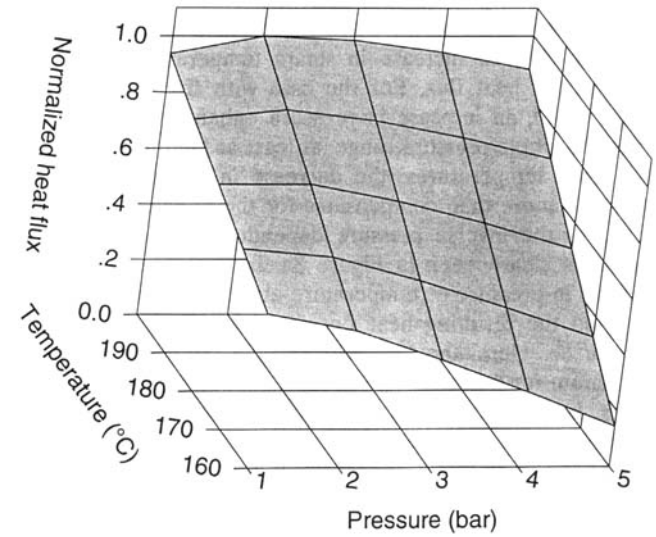

Figure 8b. Heat flux at variable slip velocity.

This leads to higher particle velocities through the dryer. The ratio between the area and volume of the tubes also decreases with the diameter, which leads to a slower reheating of the conveying steam. This is clearly seen in Figure 9, where the temperature for the doubled diameter is, on average, significantly lower. Consequently, the slip velocity, residence time, and temperature decrease if the diameter is increased. This is a well-known problem in the scale-up of pneumatic conveying dryers. This model provides a tool with which to study this phenomenon.

Feed Rate. The feed rate influences drying indirectly by affecting the steam. The flow rate was doubled in order to investigate the influence of higher solid loadings on drying, the results of which are depicted in Figure 10. The higher the particle mass loading, the larger the influence on the steam. In this case, a doubling of the feed rate did not affect the final moisture content to a large extent. It must be kept in mind, however, that high solid loadings increase the risk of plugging. The steam is affected significantly as the feed rate

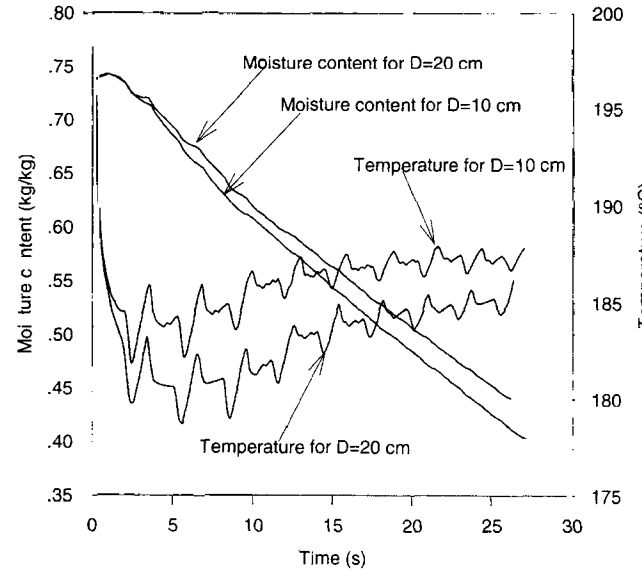

Figure 9. Effect of the dryer diameter on drying.

increases, as seen in the figure. Consequently, the average steam temperature is about 4°C lower for the high feed-rate case. The oscillations in temperature are also much larger. The net result is that the final moisture content increases when the feed rate increases. In addition to this, the energy consumption in the external heat exchangers increases.

Profiles of Moisture, Pressure, and Temperature Within the Single Wood Chip

Some interesting effects occur within the wood chips during drying under such variable drying conditions, as in this case. The temperature, moisture content, and pressure at some different points in the chip are depicted in Figure 11 as functions of residence time. The different curves represent temperature (T), pressure (P), and moisture content (M) for three different points in the chip; these points refer to the

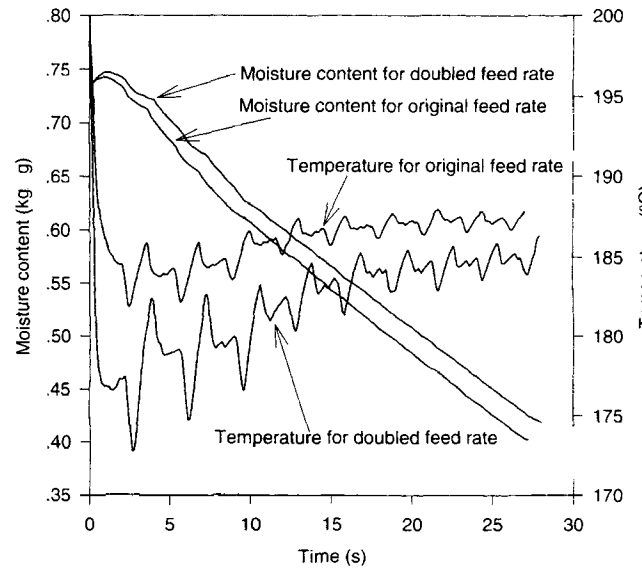

Figure 10. Effect of feed rate on drying.

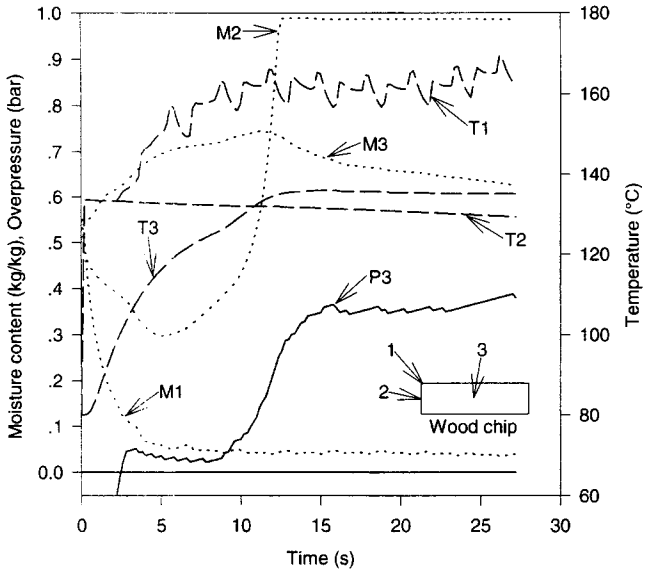

Figure 11. Temperature and pressure profiles inside the wood chip during drying.

positions indicated in the figure. Point 1 is located at the edge of the chip, point 2 at the small end, and point 3 at the center of the chip. The moisture content at point 1 (M1) decreases rapidly and then remains at a low value during the whole drying sequence. The small oscillations in this curve are due to the fact that drying intensity varies with time. The surface is actually rewetted during the periods that have a low drying rate. The temperature at the same point (T1) rises as the moisture disappears. This curve reflects the slip-velocity curve and the temperature is about 10°C lower than the surrounding steam temperature. As the surface dries out and the temperature rises, heat is conducted into the center of the chip. The temperature at the center then rises (T3). Being strongly dependent on temperature, the overpressure then starts to increase at the center as well (P3). This overpressure drives the moisture in the most permeable direction which, in this case, is the longitudinal direction. This leads to an accumulation of moisture at the small end, as illustrated by (M2). This phenomenon is discussed at length by Fyhr and Rasmuson (1996a), and is also observed both theoretically and experimentally by Perré et al. (1993). Since the moisture content at the small end is always at a high value, the temperature at this point (T2) is the saturation temperature at the prevailing pressure. The temperature decrease at this point therefore reflects the pressure drop through the dryer.

Conclusions

The hydrodynamic-dryer model presented in this article predicts temperature profile, overall pressure drop, as well as residence time that are in agreement with experimental observations. Together, the hydrodynamic and single-particle models constitute the complete dryer model, which predicted a final moisture content of bark chips that was in acceptable agreement with experiments.

The comprehensive single-particle model is necessary for the following reasons: first, to predict the heatup period where initial condensation actually increases the moisture content. Second, to model the falling-rate period, which is essential in the drying of less permeable materials such as spruce chips. Third, the pressure drop at the outlet induces flashing, which reduces the moisture content significantly.

The irregular motion and nonspherical shape of the chips mean that correlations for the heat transfer and drag coefficients based on spherical particles would be insufficient in this case. Measurements of these coefficients were performed in order to account for this. It was shown that the heat-transfer coefficients in particular differed significantly from conventional correlations.

Complex coupling effects arise when the steam properties are changed. Drying is directly affected by the heat-transfer rate and the varying residence times. Summarizing the effect of the steam properties, it can be said that the final moisture content increases when the steam temperature decreases. A rise in pressure leads to increased final moisture content, although the heat-transfer rate increases. This is due to the decreased residence time and the increased initial condensation. An increase in the steam velocity increases the final moisture content.

The chip dimensions affect drying significantly. A large chip has a higher final moisture content than a small chip, although the residence time is somewhat increased. An increase in the particle feed rate leads to a lower steam temperature in the dryer, which increases the final moisture content. A particle-size distribution did not affect drying significantly, that is, the final moisture content of the different particle sizes were the same as in the single-size calculations. The average outlet moisture content is nevertheless affected by a size distribution.

The construction of the dryer also affected drying in several ways: extending the height of the towers while keeping the total length constant reduced the residence time and increased the final moisture content; and a larger tube diameter allowed for a higher throughput of solids but, as a consequence, the residence time and steam temperature decreased, which lead to slower drying.

Notation

A = area, m^2
C_p = heat capacity, J/kg·K
D = diffusion coefficient, m^2/s
g = gravitation constant, m/s^2
H = enthalpy, J/kg
k = relative permeability
M = mass accumulation, kg/m^3; molar mass, kg/mol
Nu = Nusselt number
n = number of particles
n = mass flux, $kg/m^2 \cdot s$
Pr = Prandtl number
Q = heat accumulation, J/m^3
q = heat flux, W/m^2
Re_D = Reynolds number based on the tube diameter
Re = Reynolds number based on the diameter of a sphere with volume equal to the particle
Re_L = Reynolds number based on the length of the chip
V = volume, m^3
x = mass fraction
$\bullet$ = porosity; voidage
λ = heat conductivity, W/m·K
σ = surface tension, N/m

Subscripts and superscripts

i = particle size i
L = longitudinal

s = solid; surface
T = tangential
w = water
v = vapor
∞ = ambient
κ = component

Literature Cited

Adewumi, M. A., and H. Arastoopour, "Two-dimensional Steady State Hydrodynamic Analysis of Gas-Solids Flow in Vertical Pneumatic Conveying Systems," *Powder Technol.*, **48**, 67 (1986).

Bandrowski, J., and G. Kaczmarzyk, "Gas-to-Particle Heat Transfer in Vertical Pneumatic Conveying of Granular Materials," *Chem. Eng. Sci.*, **33**, 1303 (1978).

Berlemont, A., P. Desjonqueres, and G. Gouesbet, "Particle Lagrangian Simulation in Turbulent Flows," *Int. J. Multiphase Flow*, **16** (1), 19 (1990).

Björk, H., and A. Rasmuson, "Moisture Equilibrium of Wood and Bark Chips in Superheated Steam," *Fuel*, **74**, 1887 (1995).

Clift, R., J. R. Grace, and M. E. Weber, *Bubbles, Drops and Particles*, Academic Press, New York (1978).

Fyhr, C., and A. Rasmuson, "A Mathematical Model of Superheated Steam Drying of Wood Chips and other Hygroscopic Porous Media," *AIChE J.*, **42**, 2491 (1996a).

Fyhr, C., and A. Rasmuson, "Some Aspects of the Modelling of Wood Chips Drying in Superheated Steam," *Int. J. Heat Mass Transfer*, **40**(12), 2825 (1996b).

Gidaspow, D., *Multiphase Flow and Fluidization*, Academic Press, Orlando, FL (1994).

Haider, A., and O. Levenspiel, "Drag Coefficient and Terminal Velocity of Spherical and Nonspherical Particles," *Powder Technol.*, **58**, 63 (1989).

Hilmart, S., and U. Grén, "Steam Drying of Wood Residues—An Experimental Study," *Drying*, Hemisphere P. C., p. 210 (1987).

Kemp, C., D. E. Oakley, and R. E. Bahu, "Computational Fluid Dynamics Modelling of Vertical Pneumatic Conveying Dryers," *Powder Technol.*, **65**, 477 (1991).

Lee, S. L., and F. Durst, "On the Motion of Particles in Turbulent Duct Flows," *Int. J. Multiphase Flow*, **8**(2), 125 (1982).

Perré, P., M. Moser, and M. Martin, "Advances in Transport Phenomena during Convective Drying with Superheated Steam and Moist Air," *Int. J. Heat Mass Transfer*, **36**(11), 2725 (1993).

Pettyjohn, E. S., and E. B. Christiansen, "Effect of Particle Shape on Free-settling Rates of Isometric Particles," *Chem. Eng. Prog.*, **44**(2), 157 (1948).

Pruess, K., *TOUGH User's Guide*, Lawrence Berkeley Lab., Univ. of California, Berkeley (1987).

Ranz, W. E., and W. R. Marshall, "Evaporation from Drops," *Chem. Eng. Prog.*, **48**(3), 141; also **48**(4), 173 (1952).

Siau, J. F., *Transport Processes in Wood*, Springer-Verlag, Berlin (1984).

Sorensen, A., "Mass Transfer Coefficients on Truncated Slabs," *Chem. Eng. Sci.*, **24**, 1445 (1969).

Welty, J. R., C. E. Wicks, and R. E. Wilson, *Fundamentals of Momentum, Heat and Mass Transfer*, 3rd ed., Wiley, New York (1984).

Whitaker, S., "Forced Convection Heat Transfer Correlations for Flow in Packed Beds and Tube Bundles," *AIChE J.*, **18**, 361 (1972).

Yang, W. C., "A Correlation for Solid Friction Factor in Vertical Pneumatic Conveying Lines," *AIChE J.*, **24**(3), 548 (1978).

Appendix A: Mathematical Model for the Single Particle

All transport parameters given here are valid for sapwood of spruce or pine. Transport in two directions is included in order to account for the strong anisotropicity of wood. The longitudinal (L) direction is equal to the fiber direction in wood and the transversal (T) direction is some combination of the radial and tangential directions in wood.

The wood contains free water (X_l) above the fiber saturation point (X_{fsp}), and all water below this point is treated as bound water. The amount of free water is calculated as

$$X_l = X - X_{fsp},$$

where

$$X_{fsp} = 0.598 - 0.001T \qquad \text{(Siau, 1984)}.$$

Balance equations

Mass:

$$\frac{\partial M^\kappa}{\partial t} = \nabla \cdot \left(\sum_{\alpha = l,g} \boldsymbol{n}_\alpha x_\alpha^\kappa \right)$$

where

$$M^\kappa = \epsilon \sum_{\alpha = l,g} S_\alpha \rho_\alpha x_\alpha^\kappa,$$

where the relation between the moisture content X and liquid saturation S_l is written as:

$$X = \frac{S_l \epsilon \rho_l}{(1-\epsilon)\rho_{\text{wood}}}.$$

Heat:

$$\frac{\partial Q}{\partial t} = \nabla \cdot \boldsymbol{q}$$

where

$$Q = (1-\epsilon)\rho_{\text{wood}} Cp_{\text{wood}} T + \epsilon \sum_{\alpha = l,g} S_\alpha \rho_\alpha u_\alpha$$

$$\rho_{\text{wood}} = 1{,}500 \text{ kg/m}^3 \qquad Cp_{\text{wood}} = 1{,}400 \text{ J/kg} \cdot \text{K},$$

where porosity for soft wood is $\epsilon = 0.73$, and porosity for dense wood is $\epsilon = 0.67$.

Internal mass transfer

Convection according to Darcy's law:

$$\boldsymbol{n}_\alpha = -\rho_\alpha \frac{k_\alpha}{\mu_\alpha} K_\alpha \nabla P_\alpha.$$

Relative permeabilities (Perré et al., 1993):

$$k_{l,T} = X^{*3} \qquad \text{with} \quad X^* = \frac{X_l}{X_{\text{sat}}}$$

$$k_{g,T} = 1 + (2X^* - 3)X^{*2}$$

$$k_{l,L} = X^{*8}$$

$$k_{g,L} = 1 + (4X^* - 5)X^{*4}.$$

Absolute permeabilities (Siau, 1984):
Spruce

$$K_{l,T} = 5 \times 10^{-17}, \quad K_{l,L} = 5 \times 10^{-13}$$

Pine

$$K_{l,T} = 2.5\times10^{-16}, \quad K_{l,L} = 1\times10^{-12}$$

$$K_g = 0.1\times K_l \text{ (pit aspiration)}.$$

The liquid and gas pressures are coupled as:

$$P_l = P_g - P_c,$$

where P_c is the capillary pressure (Perré et al., 1993):

$$P_c = 1.364\times10^5\sigma(X_l + 1.2\times10^{-3})^{-0.63}.$$

Bound water diffusion (Siau, 1984):

$$\boldsymbol{n}_l^w = -D_{bw}\nabla X$$

$$D_{bw,T} = 0.05D_{BT}/((1-a^2)(1-a))$$

$$D_{BT} = 7\times10^{-2}\exp(-(9{,}200-7{,}000X)/RT)$$

$$a^2 = 1-0.5(\epsilon + X) \qquad R = 1.987 \text{ kcal/mol}\cdot\text{K}$$

$$D_{bw,L} = D_{bw,T}250a^2$$

Internal heat transfer (convection + conduction)

$$\boldsymbol{q} = \sum_{\alpha=l,g}(\boldsymbol{n}_\alpha H_\alpha) - \lambda\nabla T$$

conductivity (Perré et al., 1993):

$$X \geq 0.4, \lambda_T = (0.65/100X + 0.0932)$$
$$\times(1+3.65\times10^{-3}T)(0.986+2.695X)$$
$$X \leq 0.4, \lambda_T = (0.129-0.049X)(1+(2.05+4X)$$
$$\times10^{-3}T)\times(0.986+2.695X)$$
$$\lambda_L = 2.5\lambda_T \qquad (T \text{ in } ^\circ\text{C}).$$

Vapor pressure lowering (Björk and Rasmuson, 1995)

$$P_v = \theta P_{v,\text{sat}}$$

$$\theta = D + \sqrt{D^2 + A/B}$$

$$A = -9.94 + 2.45/X_{fsp}, \qquad B = 58.17 - 7.69/X_{fsp}$$

$$C = 68.08 - 9.15/X_{fsp}, \qquad D = -0.5(1/CX - C/B).$$

Boundary conditions

Mass:

$$P|_s = P_\infty.$$

This pressure condition is realized by setting very high permeabilities at the surface. Gas is allowed to cross the surface only. In the case of air in the surroundings, the additional mass-transfer condition is

$$n_g^w|_s = k_c\frac{M_w P}{RT}(y_{w,s} - y_{w,\infty}).$$

Heat:

$$q|_s = h(T_\infty - T_s) + \sigma e(T_\infty^4 - T_s^4) + \boldsymbol{n}_g H_g,$$

where the emissivity, e, is set to 0.9.

Appendix B: Significance of the Basset and Added-Mass Forces

The added-mass force is associated with the acceleration of fluid near particles in attaining the velocity of the particle. This added, or carried mass, for a sphere equals one-half of the displaced fluid as:

$$F_{am} = \frac{1}{2}V_p\rho_f\frac{d}{dt}(v_g - v_p). \tag{B1}$$

The Basset, or history force is more complex and only approximate expressions are available. The flow around a particle during accelerated motion is different from when it is in steady motion. The force arises from the continuous adjustment of the flow pattern and depends on the history of the motion. The Basset force is often written as

$$F_B = \frac{3}{2d_p}V_pC\sqrt{\frac{\rho_f\mu}{\pi}}\int_0^t\frac{\dfrac{d(v_p - v_g)}{d\tau}}{\sqrt{t-\tau}}d\tau, \tag{B2}$$

where C is a constant of the order of 3 (Berlemont et al., 1989). The following considerations can be made in order to evaluate the significance of these terms. They are both dependent on the relative acceleration, which, in this case, is equal to the acceleration of the single particle since the gas velocity is approximately constant. The maximum acceleration is encountered when the particle velocity is zero and can be written as

$$\left.\frac{dv_p}{dt}\right|_{t=0} = \frac{A_p}{2V_p}C_D\frac{\rho_g}{\rho_p}(v_g - v_p)|v_g - v_p| \approx 61 \text{ m/s}^2. \tag{B3}$$

The calculation is valid for a chip with the dimensions (L, W, T) = (30, 24, 4) mm, a density of 1,000 kg/m^3, a drag coefficient equal to 2.4, and a gas velocity equal to 20 m/s. It is furthermore assumed that the gravity force is negligible (inclusion of this force reduces the acceleration). The drag force on the particle is then 0.18 N, and the added mass force becomes 1.1×10^{-4} N, which is less than 0.06% of the drag force. If it is assumed that the acceleration is constant over a period of 1 s (an assumption in great favor of the Basset force), the integral in Eq. B2 can be integrated to give:

$$F_B = \frac{3}{2d_p}V_pC\sqrt{\frac{\rho_f\mu}{\pi}}2\sqrt{t}\frac{dv_p}{dt} \approx 2.2\times10^{-4}N, \tag{B4}$$

where d is taken as the diameter of a sphere with a volume equal to the chip. Again, this force is negligible when compared to the drag force (0.12%). It can be concluded, from this analysis, that both these forces can be neglected in the calculations.

Appendix C: Sensitivity Analysis for the Error in Particle–Wall Friction Factor, f_p

The drag coefficient calculated from Eq. 22 can be erroneous due to the assumed value for the wall friction coefficient. Equation 22 can be written as

$$C_D = \frac{m_p g + 0.5 f_p m_p v_p^2 / D}{0.5 A_p \rho_g v_{\text{slip}}^2}. \tag{C1}$$

Here the slip velocity and particle velocity are measured for different chip sizes and densities. The value for f_p is extracted from Eq. 20. When an error in this coefficient is introduced, the C_D value changes as in Table C1. As seen, the C_D is only affected approximately one-third of the error of f_p. The most important parameter, however, is the residence time. In fact, the residence time is unaffected by an error in f_p. If f_p is reduced, the value for C_D calculated from Eq. C1 also becomes lower. These then equalize and give the same residence time. Thus if this investigation were performed to evaluate the value for C_D only, the errors would be as in the Table C1; however, if applied to a similar system, the residence time would be unaffected. The system on which the calculated C_D is applied is the pilot dryer (Figure 1) that is similar to the small-scale pilot dryer (Figure 3) on which the experiments were performed. Thus, in conclusion it can be stated that an error in f_p is of minor importance in this case.

Table C1. Error in C_D as a Function of the Error in F_p

Error in f_p	Error in C_D
25%	8.4%
50%	17%
100%	34%

Appendix D: Radiative Contribution to the Heat Transfer

The radiative contribution to the heat transfer during the experiments for the determination of the heat-transfer coefficients is calculated according to

$$Q_{\text{rad}} = C_{12} A \sigma (T_s^4 - T_\infty^4), \tag{D1}$$

where C_{12} is dependent on the geometry and emission factors of the exchanging surfaces and σ is the Stefan-Boltzmann constant. Without going into detail in evaluating C_{12}, it was taken as 1 (an assumption in great favor of the radiative contribution). The equivalent radiative heat-transfer coefficient then ranged between 0.7 and 2% of the convective heat-transfer coefficient, which indicates that radiation has a negligible influence on the measurements in this case.

Manuscript received Oct. 21, 1996, and revision received July 9, 1997.